Environmental Science and Pollution Research (2020) 27:6088–6102
https://doi.org/10.1007/s11356-019-07329-7

RESEARCH ARTICLE

Development of an activated carbon impregnation process with iron oxide nanoparticles by green synthesis for diclofenac adsorption

Carole Silveira[1] · Quelen Letícia Shimabuku-Biadola[1] · Marcela Fernandes Silva[1] · Marcelo Fernandes Vieira[1] · Rosângela Bergamasco[1]

Received: 17 April 2019 / Accepted: 6 December 2019 / Published online: 21 December 2019

Abstract

The objective of this study was to impregnate the surface of palm coconut activated carbon with nanoparticles of iron compounds using *Moringa oleifera* leaf extracts and pomegranate leaf by a green synthesis method and to evaluate its adsorption capacity for sodium diclofenac. The adsorbent material was characterized by zeta potential, X-ray diffraction (XRD), N_2 adsorption/desorption (BET method), transmission electronic microscopy (TEM), and scanning electronic microscopy (SEM) coupled to dispersive energy spectrometry X-ray (EDX) methods. To evaluate the adsorption capacity of sodium diclofenac, the influence of pH, kinetics, isotherms, and thermodynamic properties were analysed. The impregnated adsorbents showed efficiency in the adsorption of sodium diclofenac. The kinetic model that best fit the experimental data was the pseudo-second-order model, and the equilibrium model was the Langmuir model. As for the thermodynamic study, it was verified that the adsorption reaction for all adsorbents occurs in a spontaneous, favourable way, and it is endothermic by physisorption. Therefore, this process is promising because it is a clean and non-toxic method when compared with chemical methods for the synthesis of nanoparticles.

Keywords Green synthesis · Diclofenac · Water treatment · Nanoparticles · Adsorption · Characterization · *Moringa oleifera* · Pomegranate

Introduction

Organic microcontaminants, such as drugs and endocrine disruptors, are present in surface waters due to the increased degree of pollution of bodies of water by anthropic activities. Drugs are the most widely used organic compounds in the world, with enormous benefits for the whole society. High human consumption, as well as veterinary and industrial practices, generates contamination of both surface water and groundwater with such compounds. The presence of drugs in the aqueous environment has received great attention from experts since such compounds in water represent an emerging risk, especially for aquatic biota, due to the ability of these compounds to interfere adversely in different organisms, even at very low concentrations (Kümmerer 2009). The effects may include endocrine interference, genotoxicity, and, consequently, alteration in the metabolic behaviour and functions of the species in the ecosystem (Jorgensen and Halling-Sorensen 2000).

Diclofenac (Fig. 1) is an acidic drug that belongs to the family of non-steroidal anti-inflammatory drugs. This drug is widely used in the relief of pain and inflammation; in the treatment of rheumatoid arthritis, osteoarthritis, and musculoskeletal injuries; in the prevention of intraoperative myiosis during cataract extraction; in the treatment of inflammation after laser eye surgery treatment; and in the relief of ocular signs, allergic conjunctivitis, and post-surgery analgesia in

Responsible editor: Tito Roberto Cadaval Jr

✉ Quelen Letícia Shimabuku-Biadola
le.shimabuku@gmail.com

Carole Silveira
carole_silveira@hotmail.com

Marcela Fernandes Silva
celafs@gmail.com

Marcelo Fernandes Vieira
marcelofvieira@hotmail.com

Rosângela Bergamasco
rbergamasco@uem.br

[1] Department of Chemical Engineering, State University of Maringá, Avenida Colombo, 5790. Bloco D90, Maringá, Paraná 87020–900, Brazil

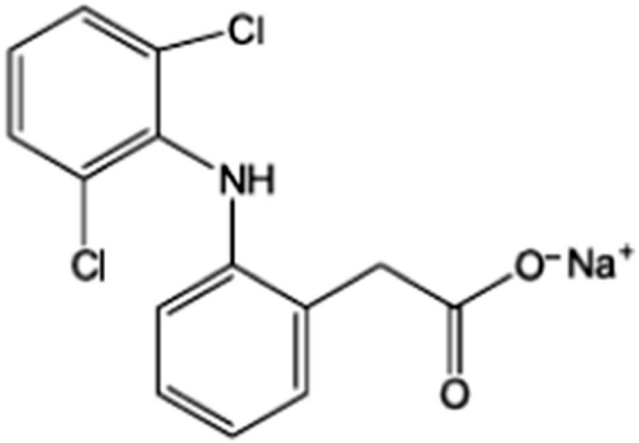

Fig. 1 Chemical structure of sodium diclofenac (DCF) (Larous and Meniai 2016)

human and veterinary medicine. Therefore, diclofenac is one of the 10 compounds most commonly found in aquatic environments due to its high level of consumption, and its percentage of removal in conventional wastewater treatment may be less than 20% (Iliescu et al. 2004; Sotelo et al. 2014), so it is very important to control its concentration in the environment. Previous studies have reported that diclofenac may cause adverse effects, such as thyroid tumours and hemodynamic changes, with chronic human exposure (Collier 2007; Schriks et al. 2010).

The conventional treatment (coagulation, flocculation, sedimentation or flotation, filtration, and disinfection) used in most water treatment plants does not present high efficiency in the removal of dissolved compounds or organic microcontaminants; thus, new techniques and complementary treatment processes are required (Choi et al. 2006; Yoon et al. 2007).

One of the processes that meets these needs is adsorption in activated carbon, which is an adsorbent composed primarily of carbon. Its structure is largely amorphous, with a small crystalline fraction. These materials have been used as adsorbents, with optimum efficiency and versatility in various applications in both liquid and gaseous phase due to their highly developed porosity and extended apparent surface area (Bansal and Goyal 2005). Combining the advantages of activated carbon with the properties of metal nanoparticles can be a promising solution to produce new materials that meet an extensive list of applications (Darezereshki et al. 2013).

Iron nanoparticles have attracted interest for the remediation and *treatment of water contaminated* by organic or inorganic pollutants due to the higher intrinsic reactivity of their superficial sites (Zhang et al. 2011). Iron oxides can be easily synthesized and have a high surface area; they are used in the preparation of different adsorbents used for the adsorption of cations, anions, organic compounds, and other substances present in contaminated water (Kobayashi et al. 2008; Gulshan et al. 2009; Zibin et al. 2019; Khatami et al. 2019).

Nanoparticles can be impregnated on the activated carbon surface by techniques commonly used in the preparation of catalysts, such as vacuum treatment (Park and Jang 2003), dry impregnation (Silva et al. 2003; Silva et al. 2006), and impregnation with excess solvent (Silva et al. 2003; Kumar et al. 2004). As vacuum treatment entails increasing production costs, dry and wet impregnation techniques are the most indicated. However, the use of common organic solvents in several methods can be harmful due to their release into process effluents or as gaseous compounds, requiring the development of less polluting techniques.

The green method is a clean, non-toxic, and low-cost method when compared with chemical methods in the synthesis of nanoparticles (Iravani 2011). Plant extracts can be used in green synthesis processes and can act as reducing agents and stabilizing agents for the development of metallic nanoparticles (Philip 2009; Thakkar et al. 2010). These extracts can be obtained from plant parts or called as residues, such as leaves; in some cases, the fruits or seeds are also used. Thus, the objective of this work was the impregnation of the surface of activated carbon with iron oxide nanoparticles using leaves of *Punica granatum* (Pomegranate) and *Moringa oleifera* by a green method to obtain characteristics more suitable for their use in the adsorption of sodium diclofenac (DCF).

Materials and methods

Preparation of extracts

Punica granatum (Pomegranate) and *Moringa oleifera* fresh leaves (Fig. 2) were selected from plants available in the city of Maringá-PR, Brazil. The extracts were prepared separately by adding 60 g of fresh leaves to 1000 mL of distilled water at 80 °C under agitation for 1 h, with posterior filtration. The use of the extract occurred after it reached room temperature. The pH values of the ready extracts were 7.1 and 6.5 for pomegranate and *Moringa oleifera*, respectively.

Determination of phenolic compounds in extracts

For characterization of the extracts of *Moringa oleifera* and pomegranate leaves, quantification of phenolic compounds by the Folin-Ciocalteu colorimetric method was performed using the methodology proposed by Singleton and Rossi (1965) and adapted by Daves (2003). Folin-Ciocalteu reagent is a solution of polymer-complex ions formed from phosphomolybdic and phosphotungstic heteropoly acids. This reagent oxidizes the phenolates, reducing the acids to a blue Mo–W complex. A standard curve of gallic acid was used for quantification of phenols. The reading was performed in triplicate using a UV-VIS HACH DR 5000 spectrophotometer with an absorbance of

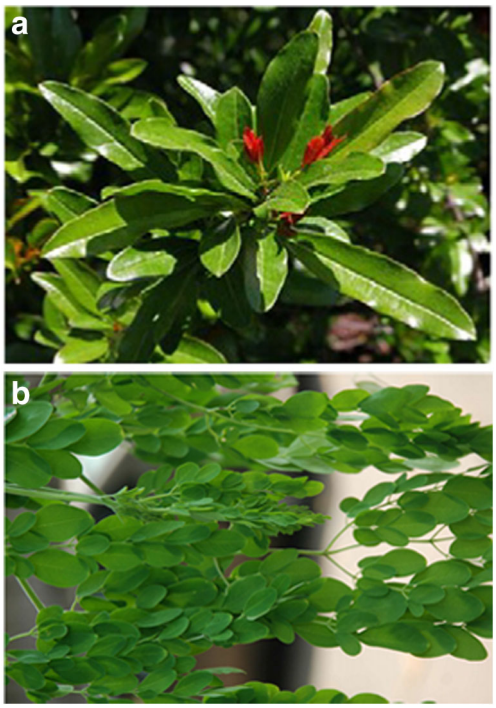

Fig. 2 Pomegranate (**a**) and *Moringa oleifera* (**b**) leaves (Olabode et al. 2015; Prasad et al. 2017)

765 nm, and the results are expressed as milligram of gallic acid per gram of leaves (mg GAE g^{-1})

Impregnation of activated carbon

Impregnation of the activated carbon with iron oxide nanoparticles was carried out using an iron concentration of 1% in relation to the activated carbon mass. The required amounts of iron nitrates [$Fe(NO_3)_3{\cdot}9H_2O$ (Neon) with 99.10% purity] were solubilized in distilled water and added to the granular activated carbon of palm coconut (Brazilian Catalyst Factory [BCF] Ltda) together with the extract of leaves [ratio of 2:1 (v/v) extract/iron nitrate solution], which were left under shaking in a bath (Dubnoff 304-TPA) for 12 h. Then, the coals were separated by filtration and dried at 323 K in a circulation and air-renewing greenhouse (Digital timer, Sterilifer). Three syntheses of each adsorbent were made and mixed for the adsorption test. The adsorbent nomenclatures used in the present work were GAC (pure granular activated carbon), GACFePo (granular activated carbon functionalized with Fe using pomegranate extract), and GACFeMo (granular activated charcoal functionalized with Fe using *Moringa oleifera* extract).

Characterization of adsorbent materials

The adsorbents impregnated with the different leaf extracts were characterized using Zeta potential, X-ray diffraction (XRD), N_2 adsorption/desorption (BET method), transmission electronic microscopy (TEM), and scanning electronic microscopy (SEM) coupled to X-ray dispersive energy spectrometry (XDE) methods.

The zeta potential of the adsorbents was evaluated as a function of media pH (5, 7, and 10) by electrophoretic light dispersion using a Beckman Coulter Delsa (TM) Nano Zeta Potential Analyzer.

The diffractograms of the samples were obtained by XRD using a diffractometer Bruker-AXS D8 Advance model with CuKα radiation ($\lambda = 0.154$ nm) and 2θ scan ranging from 15° to 70° with 2° min^{-1} step. The diffractograms were interpreted using the MDI software database (Jade 5 XRD Pattern Processing & Identification, version 5.0.0.37), and the size of the crystallites was estimated by the Scherrer equation (Eq. 1). At the peak of $2\theta = 20.50°$, in which 0.89 is the Scherrer constant related to a spherical shape approximation, λ is the wavelength of the radiation, B is the width of the peak at half height, and θ_B is the Bragg angle (Koch et al. 2007).

$$d = \frac{0.89\lambda}{(B\cos\theta_B)} \quad (1)$$

The texture characteristics of the samples were estimated by adsorption/desorption of nitrogen (N_2) at 77 K in a gas sorption system (Quantachrome Autosorb 1® volumetric analyser). Specific surface area (S_{BET}), micropore area (S_{micro}), average pore diameter (D_p), total pore volume (V_P), micropore volume (V_{micro}), mesopore volume (V_{meso}), and the adsorption/desorption isotherms were obtained.

The surface morphology of the samples was evaluated by the SEM technique, with micrographs generated by topographic contrast through the scanning electron microscope (Shimadzu SS-550 SuperScan SEM), with 15.0 kV acceleration voltages that has coupled a system of dispersive energy spectroscopy of X-ray, which provides a spectrum of the chemical elements present in the analysed sample and also by TEM, using JEOL JEM-1400 electron microscope with 120 kV.

Adsorption tests

To investigate the pH effect on the DCF adsorption process in GAC, GACFePo, and GACFeMo, solutions of the contaminant with pH values of 5, 7, and 10 were separately prepared using 0.5 mol L^{-1} NaOH (Andirol) and 0.5 mol L^{-1} HCl (Andirol) for the adjustment and the initial concentration of 100 mg L^{-1} of DCF (purity 99–101%, Infinity Pharma). Subsequently, 50 mL of each of these solutions was added in closed containers containing 120 mg of dry adsorbent, and then, were left under shaking in a bath Dubnoff (304-TPA) at a controlled temperature and rotation (323 K and 130 rpm, respectively). Afterwards, aliquots of the

supernatant were removed, and the final contaminant concentration was analysed in a UV-VIS HACH DR 5000 spectrophotometer. The amount of adsorbed contaminant is determined in Eq. 2.

$$q_e = \frac{V_{\mathrm{Sol}}(C_0 - C_e)}{m_{\mathrm{ads}}} \quad (2)$$

where q_e is the equilibrium concentration of the contaminant in the solid phase (mg g^{-1}), V_{Sol} is the volume of solution (L), C_0 is the initial concentration of the contaminant in the solution (mg L^{-1}), C_e is the contaminant concentration at equilibrium (mg L^{-1}), and m_{ads} is the adsorbent mass (g).

The adsorption kinetics were performed using aqueous solution of DCF at the optimal pH previously determined, with a concentration of 100 mg L^{-1} and a mass of 120 mg of adsorbent. Assays were conducted using closed containers and left in a 323 K bath with shaking at 130 rpm. For determination of equilibration time, the samples were taken at predetermined time intervals (0 to 480 min) and the final solution concentration was determined at each point.

To evaluate the adsorption isotherms, the same agitation and pH value of the kinetic test were used, varying the temperature to 298, 308, and 318 K. To determine the experimental data, 50 mL of DCF solution, with an initial concentration varying from 100 to 300 mg L^{-1}, was added to closed containers with an adsorbent mass of 120 mg. The samples were shaken until the equilibrium time was reached for each adsorbent. The final adsorbate concentration was analysed.

Results and discussion

Characterization of extracts

Analysis of phenolic compounds was done to characterize the extracts used in this study, and the results are given in Table 1. Phenolic compounds are components present in leaves that act as reducing agents of nanoparticles, and they have emerged as substitutes for chemical synthesis (Njagi et al. 2010; Huang et al. 2014). According to the results presented in Table 1, both extracts showed the presence of phenolic compounds. The levels of phenolic compounds obtained in this study were also compared with other studies present in the literature for aqueous extracts. It was found that the pomegranate leaf extract had a higher concentration than the *Moringa oleifera* leaf extract.

The differences between the phenolic obtained for pomegranate and *Moringa* leaf extracts compound results presented in the table are due to the variations in the extraction techniques used, the chemical and genotypic composition of the plant, the variety, the soil type, the place of origin, the harvest season, the maturation, and the storage method (Fadavi et al. 2005; Viuda et al. 2010).

Characterization of adsorbent materials

The X-ray diffractograms presented in Fig. 3 were used to determine the structural/compositional characteristics of the produced samples. GAC was used as a reference in comparison with the other samples. The extended peaks observed in the region of 20 to 27° are considered to be from the amorphous nature of carbon (Zhang et al. 2004), suggesting a more disordered structure of the carbonaceous matrix. It is possible to observe in samples GACFePo and GACFeMo the presence of the orthorhombic phase of the iron oxyhydroxide α-FeOOH (goethite), according to the crystallographic data sheet JCPDS 29-0713 (Hockridge et al. 2009), at values of $2\theta = 20.5°$, 36.8°, 45.4°, 57.5°, and 62.8°, respectively, for crystallographic planes 101, 301, 111, 401, and 212. Shahwan et al. (2011) also found goethite when they synthesized iron nanoparticles (from $FeCl_2$) using green tea leaves.

The average diameters for the crystallites of the identified goethite phase impregnated in the activated carbon were estimated by the Scherrer equation (using the peak at 2θ equal to 20.50°), obtaining values of 91.99 nm for GACFePo and 99.72 nm for GACFeMo. These results are in agreement with that presented by Shahwan et al. (2011), who obtained goethite nanoparticles with sizes between 40 and 60 nm (verified by TEM) using the green synthesis method (but without the presence of an activated carbon matrix). It can then be observed that the proposed method was efficient for the impregnation of coal with iron oxyhydroxide nanoparticles, thus demonstrating the functionality of the obtained material. The low intensity and broad lines of the XRD peaks for the α-

Table 1 Concentration of phenolic compounds obtained for the characterization of pomegranate leaf extracts and *Moringa **oleifera***

Plant	Part of the plant	Concentration of the extract	Phenolic compounds (mg GAE g^{-1})	Reference
Pomegranate	Fresh leaves	60 g L^{-1}	44.85 ± 0.89	This work
Moringa oleifera	Fresh leaves	60 g L^{-1}	11.02 ± 0.33	This work
Moringa oleifera	Dried leaf powder	500 g L^{-1}	80	(Vyas et al. 2015)
Moringa oleifera	Dried leaves	200 g L^{-1}	29.2	(Jimoh 2018)
Pomegranate	Dried leaves	100 g L^{-1}	9.85	(Elfalleh et al. 2011)

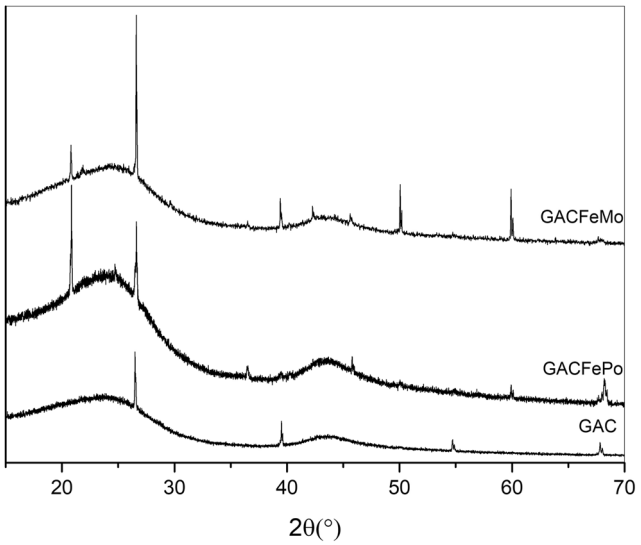

Fig. 3 X-ray diffractograms of granular activated carbon (GAC) and impregnated adsorbents

FeOOH nanostructure may be attributed to the presence of organic molecules and low-crystallization in the precursors.

The adsorption/desorption isotherms of N_2 are shown in Fig. 4. According to the *International Union of Pure and Applied Chemistry (*IUPAC) classification (Thommes et al. 2015), the adsorbents used present type I isotherms, confirming the microporous character of the adsorbent materials and indicating that adsorption occurs in monolayers with relatively small external areas and a highly developed internal area. Still, according to the authors, these characteristics are present in materials such as activated carbon. Wiśniewska et al. (2017) also obtained microporous activated carbon using biomass residue (cherry), as well as Nasri et al. (2014), who used activated carbon obtained from palm coconut.

The textural characterization parameters of the adsorbent materials (Table 2) show that after functionalization of the activated carbon surface reduction of the specific surface area (S_{BET}) and micropore area (S_{mic}) occurred.

According to Goscianska et al. (2012), this phenomenon can be justified because part of the pores of the activated carbon structure are totally and/or partially blocked by the iron oxide nanoparticles formed during impregnation of the metallic compounds, thus reducing their original characteristics (specific surface area and micropore area). Lam and Hu (2003) modified the activated carbon with Cu and the deposition of the metal in the pores occurred. According to these authors, obstruction can occur both externally and internally to the pores. The specific surface area decreases by about 5% with impregnation of the goethite nanoparticles with the Po extract and it decreases by approximately 35% with the use of the Mo extract. However, as observed in the XRD data, the sizes of the obtained crystallites are very similar; therefore, it is not possible to relate the decrease in the area with the size of the nanoparticles obtained. Thus, it is proposed that Mo

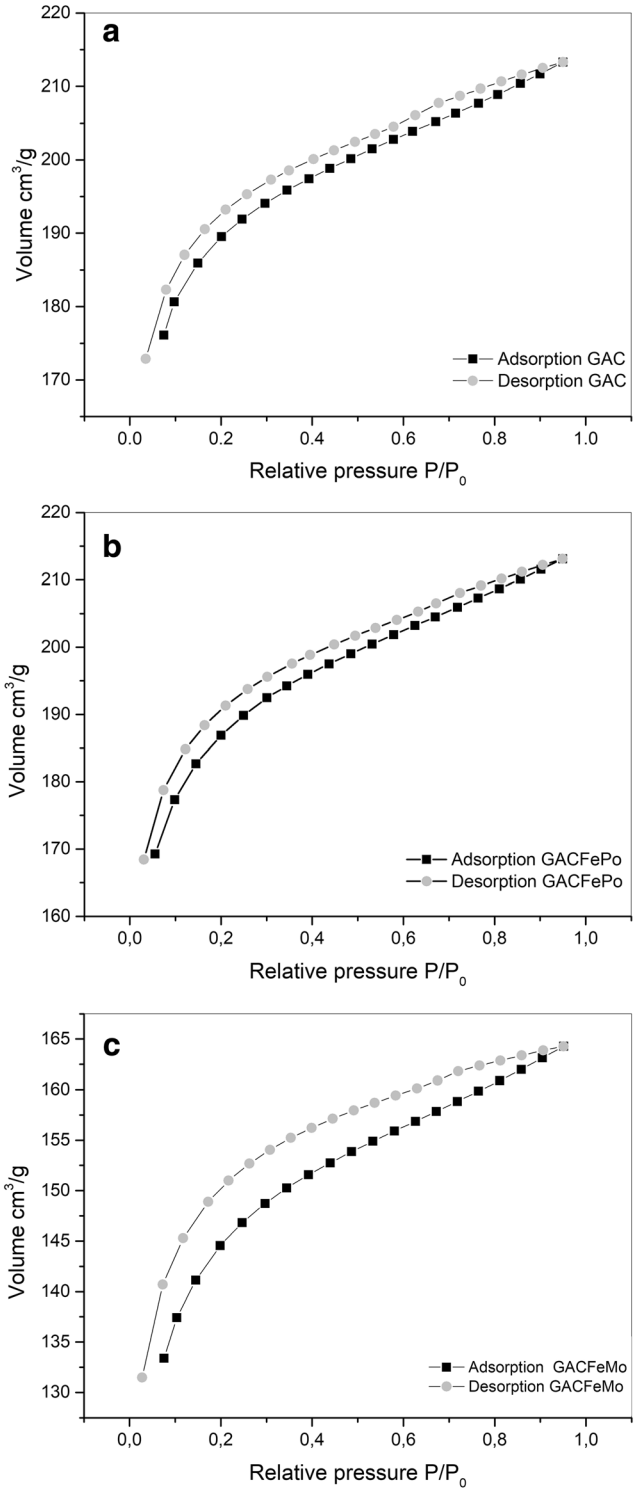

Fig. 4 BET N_2 adsorption–desorption isotherm for **a** GAC, **b** granular activated carbon functionalized with Fe using pomegranate extract (GACFePo), and **c** granular activated charcoal functionalized with Fe using *Moringa oleifera* extract (GACFeMo)

extract, due to its lower concentration of polyphenols, acts less effectively as a chelating agent with Fe ions in the formation of nuclei of the nanoparticles, as well as capping agent in

Table 2 Textural characterization parameters of GAC, GACFePo, and GACFeMo

Samples	S_{BET} ($m^2\ g^{-1}$)	S_{mic} ($m^2\ g^{-1}$)	D (nm)	V_p ($cm^3\ g^{-1}$)	V_{mic} ($cm^3\ g^{-1}$)	V_{meso} ($cm^3\ g^{-1}$)
GAC	669	469	0.98	0.329	0.287	0.039
GACFePo	639	386	1.03	0.329	0.283	0.037
GACFeMo	422	283	1.20	0.254	0.219	0.022

the interaction of these nanoparticles with the activated carbon, thus allowing for greater interaction between the nanoparticles and the surface of the activated carbon, leading to a marked decrease in the surface area. In studies of the interaction of cadmium by biochar in the presence of citrate as a capping agent, it was observed that in higher concentrations of citrate, there was a lower interaction between cadmium and biochar, resulting from the solution-phase complexation of Cd by citric acid (Uchimiya 2014). The micropore volume was predominant in the samples. A small mesopore volume was observed through the BJH method (V_{meso}) for the small volume ratio for mesopores (from 8 to 12% of the V_p) in comparison with the volume related to the micropores (from 84 to 86% of V_p); the samples can be considered as microporous. The mean diameter of micropores of all samples was less than 2 nm, thus confirming that the adsorbents are predominantly microporous. It can also be observed that impregnation of the activated carbon with goethite did not alter its microporous characteristics. Through the photomicrographs obtained by SEM (Fig. 5), the external morphology of the adsorbents can be verified.

After impregnation of the activated carbon (Fig. 5b, c), it is possible to observe particle agglomeration on the surface of the adsorbent when compared with the GAC (Fig. 5a). According to Wang et al. (2015), the agglomerate present on the surface of the activated carbon after impregnation refers to the nanoparticles of metal oxy-(hydr)oxide compounds, as was also observed by Rai et al. (2015). It should also be pointed that from Fig. 5 a, b, and c results, it can be shown the pore structure characteristics of large aperture (> 50 nm, mostly in the several micrometers in diameter) are more obvious after the impregnation (Fig. 5b, c).

The presence of α-FeOOH nanoparticles in the modified adsorbents (GACFePo and GACFeMo) can be demonstrated by X-ray dispersive energy spectroscopy (Fig. 5e, f), where carbon, oxygen, and silica from GAC can also be observed (Fig. 5d). The gold found in the samples is due to the process of metallization of the samples, necessary to perform the analysis. The size, morphology, and nanostructures of the samples were observed by TEM (Fig. 6).

Due to the contrasting difference, α-FeOOH nanoparticles can be seen as dark spots superimposed on the activated carbon surface (Srinivasan et al. 2013; Venkata Ramana et al. 2013). In the pure coal sample, only the morphology of the activated carbon (Fig. 6a) is observed, as expected. Micrographs of the activated carbon samples with α-FeOOH nanoparticles showed that the crystallites had an average diameter of less than 100 nm, which is in agreement with the results obtained in the X-ray diffraction analysis.

The zeta potential verifies the charge variation on the surface of the adsorbent as a function of the pH. The effect of different pH values on the zeta potential of the adsorbent particle suspension and the DCF solution is shown in Fig. 7.

Figure 7 shows that GAC has negative charges for the entire pH range studied. These negative charges can be attributed to the presence of functional groups, such as carboxylates and hydroxyls (Islam et al. 2016), for the pH range studied. For DCF, at pH values lower than its pKa (4.20) it is in its neutral form, decreasing its solubility in water. DCF is ionized with negative charges at pH values between 4.2 and 10; therefore, it is negative throughout the study range (Boukhalfa et al. 2017) due to the high content of electronegative groups, such as Cl and carboxylic acids, as can be observed in the structure of the molecule (Fig. 1). This generates a repulsion force between the adsorbate and adsorbent (GAC), thus explaining the lower adsorption capacity for this adsorbent. However, GACFePo and GACFeMo present positive charges in acid medium and zero load points (PCZ) at pH value close to 7.5 for both adsorbents impregnated with Fe, while in basic environments the surface becomes negative due to the dissociation of Fe–OH followed by the formation of $Fe^{-}O^{-}$ (Schwertmann and Cornell 2008). This behaviour is similar to that found by Santos et al. (2016), who synthesized iron oxide nanoparticles for use in the treatment of water. It is important to note that negative, positive, and neutral functional groups can coexist on the surface of the iron oxide. The $FeOH_2^+$ groups predominate over the FeO^- groups at pH < PCZ, that is, although the surface has a liquid positive charge, some FeO^- are still present. In the PCZ, the charges due to the $FeOH_2^+$ groups are neutralized by the presence of the negative charges of FeO^- groups and functional groups of the activated carbon, and as the pH increases, the number of FeO^- groups increases, making the zeta potential of the adsorbents more negative (Cornell and Sshwertmann 2003).

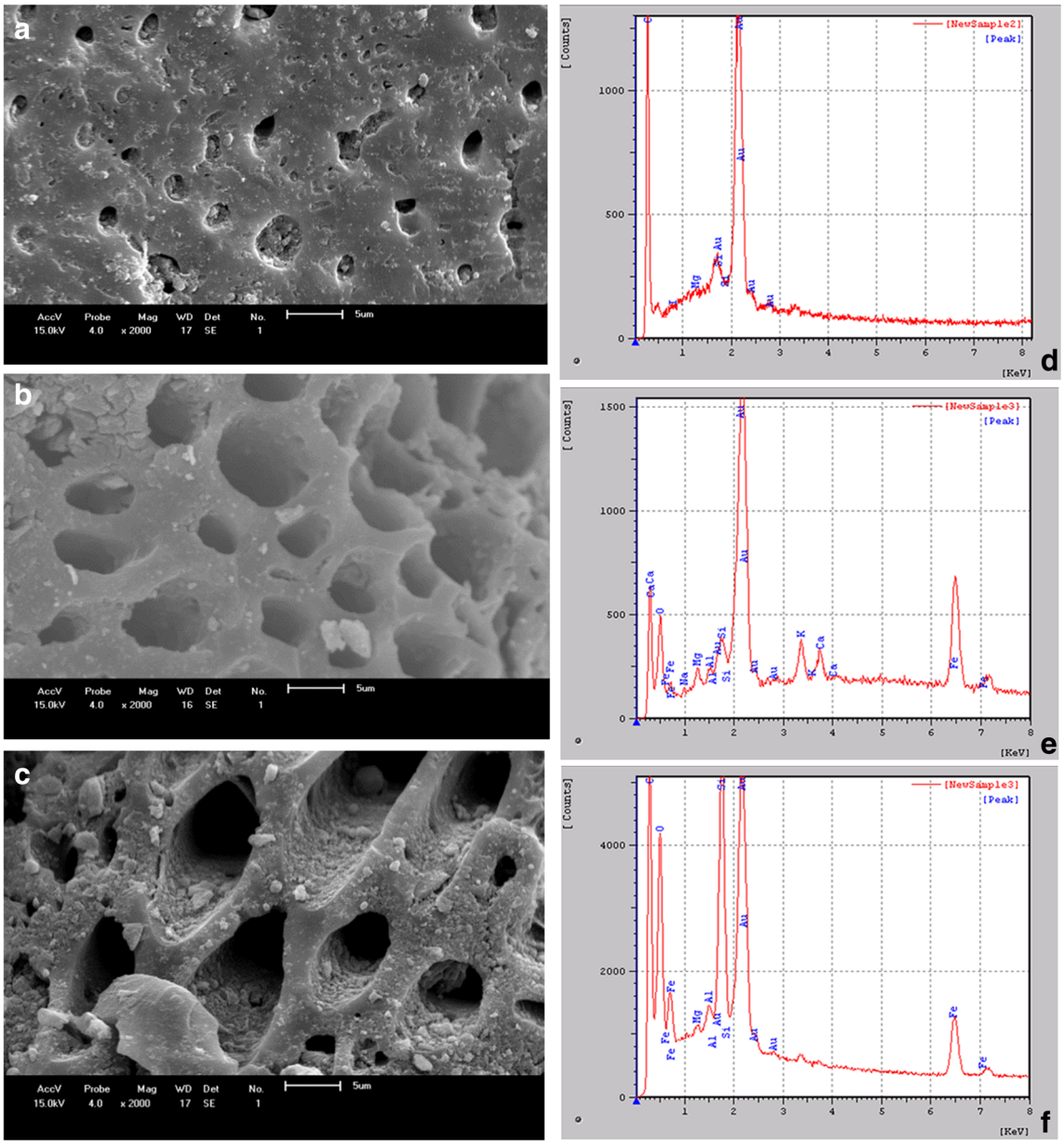

Fig. 5 Scanning electron microscopy (SEM) micrographs of **a** GAC, **b** GACFePo, and **c** GACFeMo, and X-ray dispersive energy (XDE) spectroscopy of **d** GAC, **e** GACFePo, and **f** GACFeMo

Adsorption tests

Effect of adsorption pH

The precipitation of DCF at pH values lower than its pKa (4.20) was observed and, therefore, the study was performed in the pH range above the pKa value, as shown in Fig. 8.

It is possible to observe that the adsorbents GACFePo and GACFeMo had better adsorption capacity at pH 7 (47.16 and 39.26 mg g^{-1} respectively) when compared with GAC (17.82 mg g^{-1}). Also, it can be observed that sample GACFePo, obtained using the pomegranate extract, presented higher adsorption capacity than GACFeMo, obtained with *Moringa* extract. This difference can be explained by the different contents of phenolic compounds present in these extracts (Table 1), where the pomegranate extract has a concentration approximately four times higher than the *Moringa oleifera* extract. Also, another factor that may be related to the different adsorption capacities is the BET surface area, which is superior for GACFePo in comparison with GACFeMo.

The best adsorption capacity observed at neutral pH for iron-modified adsorbents occurs because of the electrostatic attraction between the surface of the adsorbent that is positively charged, as observed by the zeta potential analyses (Fig. 7), and the DCF molecules negatively charged. As the pH

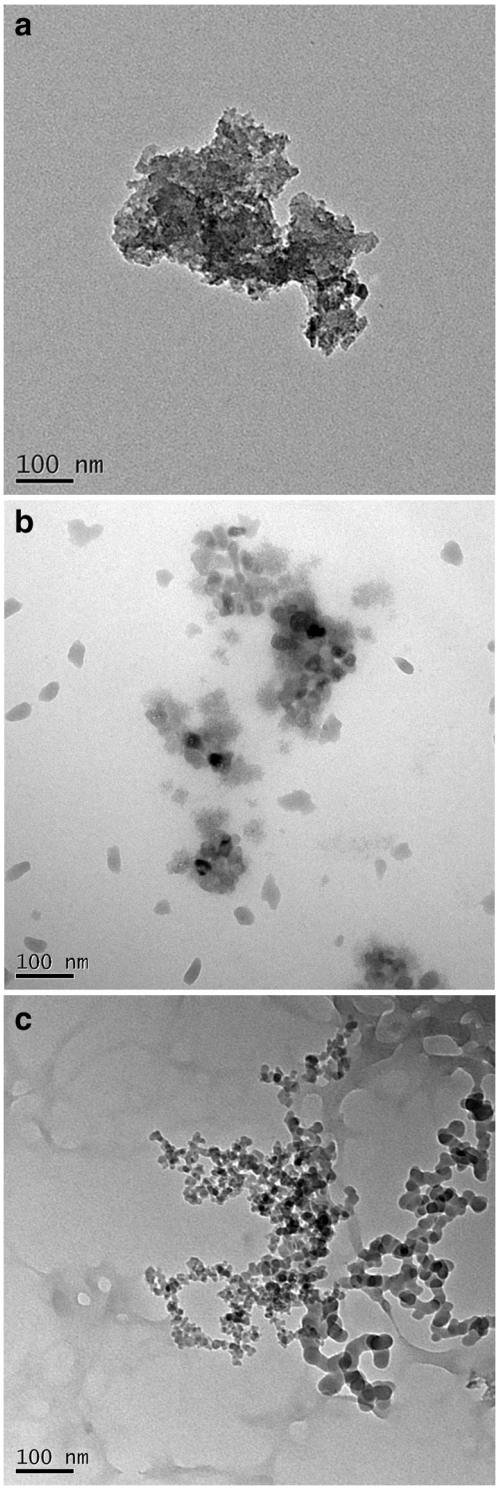

Fig. 6 Micrographs obtained by transmission electron microscopy (TEM) of **a** GAC, **b** GACFePo, and **c** GACFeMo

increases, the surface of the coal becomes negatively charged, causing electrostatic repulsion with DCF molecules, significantly reducing the amount of DCF adsorbed. It has also been reported that the decrease in DCF adsorption can be attributed to the increased mobility and solubility of DCF under alkaline

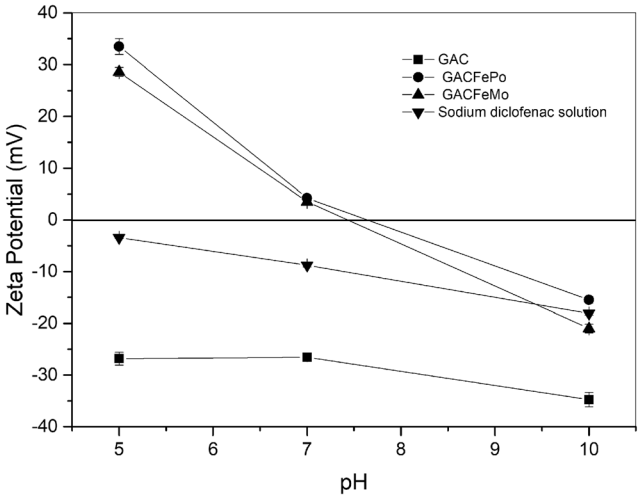

Fig. 7 Zeta potential of DCF solution and the impregnated adsorbents in relation to the pH of the medium

conditions (Zhang et al. 2018). Zhao et al. (2017) observed the same behaviour using commercial goethite in DCF adsorption, where at pH 7, there was higher removal capacity than that observed at pH 9. It should be noted, however, that these authors, using commercial goethite as adsorbents, obtained a maximum removal capacity of approximately 25 μg g^{-1}, that is, values much lower than those obtained in the present study, thus indicating that the use of an activated carbon matrix for impregnation of iron oxide nanoparticles is an extremely interesting alternative.

Adsorption kinetics

The adsorption equilibrium points were determined to evaluate the effect of contact time on DCF adsorption on GAC, GACFePo, and GACFeMo. To better understand the DCF adsorption process, the kinetic models of pseudo-first-order

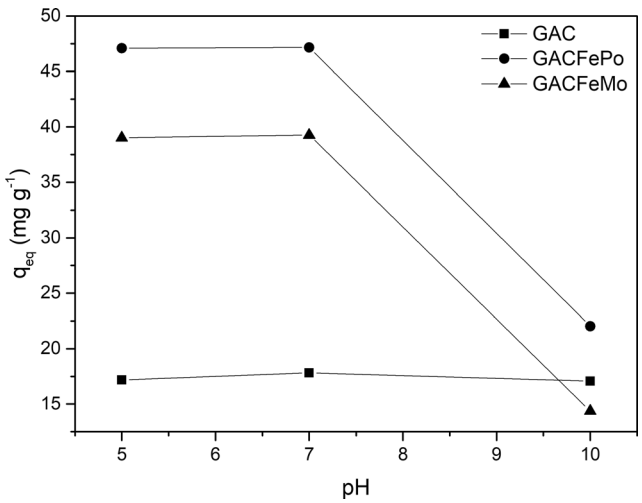

Fig. 8 Effect of solution pH on DCF adsorption using GAC, GACFePo, and GACFeMo

(Largergren 1898) and pseudo-second-order (Ho et al. 2000) in their nonlinear forms (Eqs. 3 and 4, respectively) were fitted to the experimental data and are represented in Fig. 9.

$$q_t = q_e\left(1-\exp^{-k_1 t}\right) \quad (3)$$

$$q_t = \frac{K_2 q_e^2 t}{1 + K_2 q_e t} \quad (4)$$

K_1 is the first-order constant, K_2 is the pseudo-second-order rate, q_e is the adsorption capacity at equilibrium, and q_t is the amount of DCF adsorbed at time t. The parameters of abovementioned models and the ratio coefficients for DCF adsorption are shown in Table 3.

The adsorption kinetics presented in Fig. 9 show that for the three adsorbents studied at the beginning of the process, adsorption occurs faster because a large number of active sites are available, and with the passage of time adsorption proceeds at a slower rate due to the number of decreasing empty sites, until equilibrium is reached. GAC showed an adsorption capacity of 19.68 mg g^{-1} with a contact time of 360 min, while the adsorbent impregnated with iron oxide showed an increase in the adsorption capacity, reaching values of 46.78 mg g^{-1} and 39.19 mg g^{-1}, with a contact time of 240 and 390 min for GACFePo and GACFeMo, respectively. It can be assumed that the higher adsorption capacities of the GACFePo and GACFeMo samples are due to possible interactions between DCF molecules and iron oxide. Moreover, the greater capacity of GACFePo in relation to GACFeMo can be related to the quantities of phenolic compounds identified in these different extracts (Table 1), which possibly cause the formation of different amounts of impregnated nanoparticles in the adsorbents. The correlation coefficients and parameters of the kinetic models for DCF adsorption are presented in Table 3.

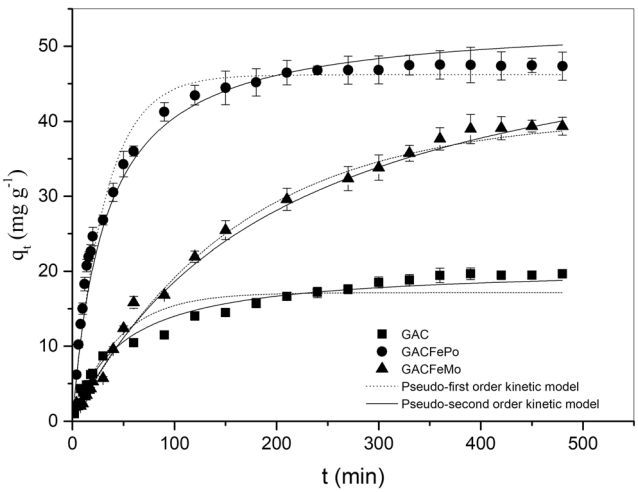

Fig. 9 Adsorption kinetics of DCF by GAC, GACFePo, and GACFeMo. Experimental and simulated by the pseudo-first-order and pseudo-second-order models

Table 3 Kinetic parameters of DCF adsorption

Kinetic model	Adsorbent		
	GAC	GACFePo	GACFeMo
$q_{eq(experimental)}$ (mg g^{-1})	19.6800	46.7800	39.1950
Pseudo-first-order model			
K_1 (1 min^{-1})	0.0149	0.0063	0.00634
q_{eq} (mg g^{-1})	18.5127	46.0813	41.0104
R^2	0.97	0.98	0.99
Pseudo-second-order model			
K_2 (g min^{-1} mg^{-1})	8.3909×10^{-4}	8.6600×10^{-4}	9.5346×10^{-5}
q_{eq} (mg g^{-1})	21.5317	50.5630	55.7185
R^2	0.98	0.99	0.99

According to the parameters presented in Table 3, both kinetic models were adjusted for the adsorption processes of DCF in all adsorbents studied, with a correlation coefficient ranging from 0.97 to 0.99. However, the experimental q_{eq} values and the derived q_{eq} values of the models showed that the q_{eq} values derived from the pseudo-second-order model are closer to the experimental q_{eq} values for the three adsorbents studied, indicating that the pseudo-second-order model was better fitted to the experimental data. It is thus assumed that the rate of reaction is dependent on the amount of solute adsorbed on the surface of the adsorbent and the amount adsorbed at equilibrium, and it is generally associated with cases where the adsorption/desorption rate controls the adsorptive process as a whole, behaving like a chemical reaction (Ho et al. 2000; Dos Santos et al. 2019). In the already mentioned study of Zhao et al. (2017), who evaluated the adsorption of sodium diclofenac in goethite, the equilibrium was reached in 480 min and the experimental data also had a better adjustment by the pseudo-second-order model.

Table 4 presents the comparison of DCF adsorption capacity at equilibrium for different adsorbents, reported in the literature, emphasizing those adsorbents similar to the one used in this study, such as activated carbon of agro-industrial residues and iron oxide in the goethite phase. It can be observed that the values found in the present study are much higher than previously reported, thus indicating the efficiency of the adsorbents produced for the purpose.

Equilibrium tests

The adsorption isotherm is important to better understand the mechanism of interactions between DCF and the adsorbents used in this study. The experimental data were obtained at three temperatures (298, 308, and 318 K), varying the initial concentration of DCF solution from 10 to 100 mg L^{-1} in order to reach equilibrium, and finally adjusting to the isotherms of Langmuir and Freundlich (Limousin et al. 2007). The models

Table 4 Amount of DCF adsorbed (q_{eq}) by some studied adsorbents from water

Material	q_{eq} (mg g^{-1})	Parameters	Reference
GAC	19.68	t = 6 h C_0 = 100 mg L^{-1} D = 2.4 g L^{-1} T = 323 K S = 130 rpm	This work
GACFePo	46.78	t = 4 h C_0 = 100 mg L^{-1} D = 2.4 g L^{-1} T = 323 K S = 130 rpm	This work
GACFeMo	39.19	t = 6.5 h C_0 = 100 mg L^{-1} D = 2.4 g L^{-1} T = 323 K S = 130 rpm	This work
Activated carbon obtained from Olive stones	3.2	t = 3 h C_0 = 20 mg L^{-1} V = 500 mL pH = 4.2 D = 5 g L^{-1} T = 296 K	(Larous and Meniai 2016)
Biochar pinewood residue	0.11	t = 4.5 h C_0 = 500 μg L^{-1} D = 2 g L^{-1} V = 50 mL S = 200 rpm T = 25 °C pH = 6.5	(Lonappan et al. 2018)
Biochar pig manure residue	0.24	t = 4.5 h C_0 = 500 μg L^{-1} D = 2 g L^{-1} V = 50 mL S = 200 rpm T = 25 °C pH = 6.5	(Lonappan et al. 2018)
Activated carbon from tissues of *Cyclamen persicum* tubers	14	C_0 = 30 mg L^{-1} V = 50 mL t = 2 h T = 298 K pH = 4 D = 5 g L^{-1}	(Jodeh et al. 2016)
Goethite (commercial)	0.03	C_0 = 1 mg L^{-1} V = 20 mL pH = 5.26 D = 20 g L^{-1} T = 298 K t = 8 h S = 175 rpm	(Zhao et al. 2017)

t time, C_0 initial concentration of DCF, D dosage of adsorbent, T temperature, S stirring

are presented in Eqs. 5 and 6, respectively. The Langmuir isotherm model is based on the assumption that each adsorption site can hold only one adsorbate molecule. The Freundlich isotherm model is commonly used to describe the adsorption characteristics for heterogeneous surfaces (Zhang et al. 2018).

$$\text{Langmuir model } q_e = \frac{q_m \times K_L \times C_e}{1 + K_L \times .C_e} \quad (5)$$

$$\text{Freundlich model } q_e = K_F \times C_e^{\frac{1}{n}} \quad (6)$$

Here, q_e is the amount of DCF adsorbed per mass of adsorbent (mg g^{-1}), C_e is the DCF equilibrium concentration (mg L^{-1}), q_m is the mass of adsorbed DCF required to completely form a monolayer of the adsorbent (mg g^{-1}), K_L is the Langmuir constant linked to the adsorption capacity (L mg^{-1}), K_F is the Freundlich constant related to the adsorption capacity (mg g^{-1})

$(L\ mg^{-1})^{1/n}$, and $1/n$ is the experimental constant representing the intensity of adsorption.

The isotherms and the respective models fitted to the data are shown in Fig. 10, while the calculated parameters for such isotherms are shown in Table 5. For all three adsorbent samples, the adsorption capacity of DCF increased with increasing equilibrium concentration (C_e). Furthermore, compared with GAC, GACFePo and GACFeMo had a higher adsorption capacity for nearly all equilibrium concentrations, which suggested that functionalization of iron oxide was beneficial for the removal of DCF from aqueous solution.

As listed in Table 5, compared with the Freundlich model, the Langmuir model fitted the adsorption isotherms of DCF onto three adsorbents better at the lower temperature (298 K), which suggested that the adsorption of DCF onto the activated carbon was probably monolayer molecular adsorption at this temperature. Moreover, the calculated values of R_L given in Table 5 are all between 0 and 1, indicating a favourable adsorption process (Qin et al. 2017).

When increasing the temperature, there is a tendency for the adsorption to be better adjusted by the Langmuir model. As can be seen, both models have very close regression values for certain temperatures, which shows that the data can fit both models. Furthermore, $1/n$ is a constant indicative of adsorption intensity or surface heterogeneity. As shown in Table 5, the values of $1/n$ for all tested adsorbents were less than 1.0, indicating that the adsorption DCF onto GAC, GACFePo, and GACFeMo was favourable.

Although the process of incorporation of iron oxide nanoparticles decreased the specific surface area of activated carbon (shown in Table 2), the adsorption efficiency was enhanced due to the interaction between iron oxide and DCF (Zhang et al. 2018).

Adsorption thermodynamics

The enthalpy variation ($\Delta H°$), system entropy variation ($\Delta S°$), and Gibbs free energy variation ($\Delta G°$) were determined from the variation of the equilibrium constant of the adsorption process for DCF with the temperature and were calculated by Eqs. 7, 8, and 9 (Al-Hakeim et al. 2014).

$$\Delta G° = -\mathrm{RT}\ \ln k_d \tag{7}$$

$$\Delta G° = \Delta H° - T\Delta S° \tag{8}$$

$$\ln K = \frac{\Delta S°}{R} - \frac{\Delta H°}{R}\ \frac{1}{T} \tag{9}$$

$\Delta G°$ is the Gibbs free energy variation, $\Delta H°$ is the enthalpy change, $\Delta S°$ is the entropy variation, R is the universal constant of ideal gases (8.314 J mol^{-1} K^{-1}), T is the absolute temperature in K, and k_d is the distribution coefficient. The value of k_d is calculated by Eq. 10, where 0.12 represents the adsorbent mass and 0.05 represents the volume of DCF, solution used in the process of adsorption (Al-Hakeim et al. 2014).

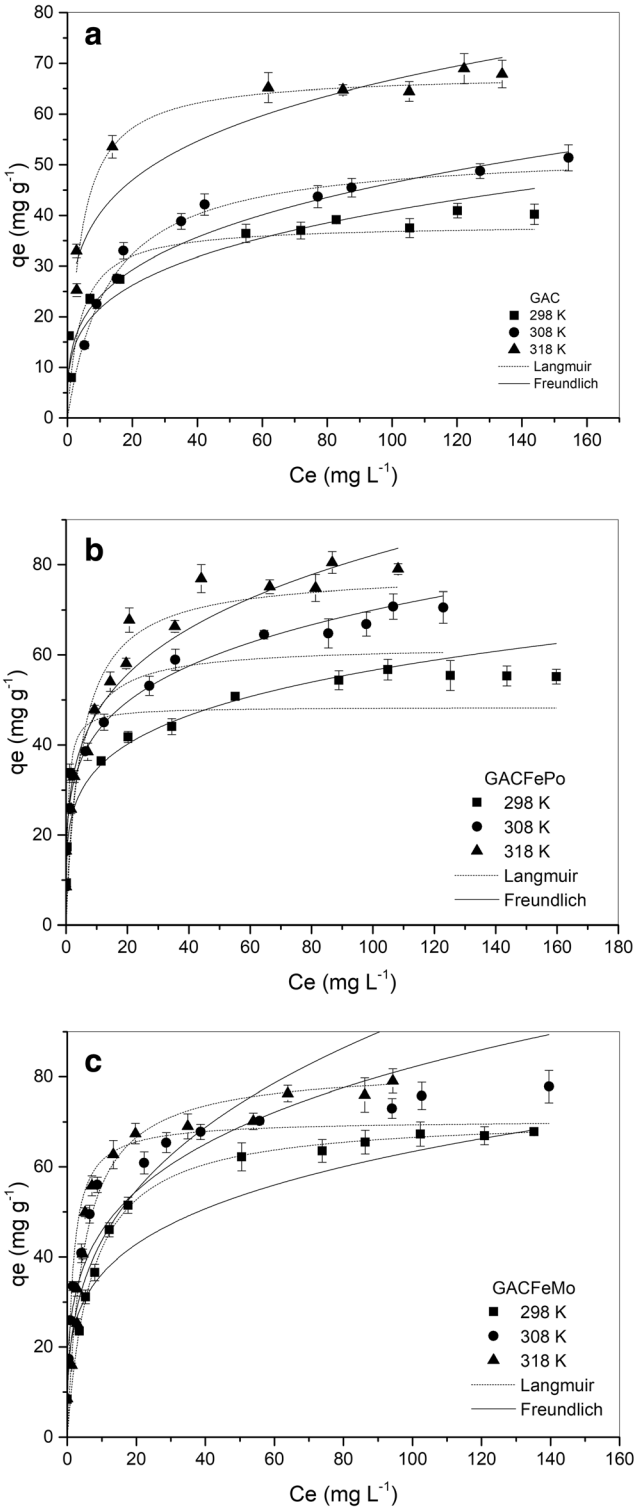

Fig. 10 Adsorption isotherms obtained at 298, 308, and 318 K for the adsorption of DCF in the adsorbents **a** GAC, **b** GACFePo, and **c** GACFeMo. Experimental conditions included an adsorbent dosage of 2.4 g L^{-1}, stirring at 130 rpm, and a pH value of 7

Table 5 Parameters obtained for the Langmuir and Freundlich isothermal models

Sample			Langmuir			Freundlich		
	T (K)	q_m	K_L	R_L	R^2	K_F	$1/n$	R^2
GAC	298	39.647	0.252	0.0910	0.91	14.434	0.216	0.96
	308	53.497	0.078	0.1933	0.97	13.429	0.273	0.96
	318	68.012	0.259	0.0537	0.99	27.098	0.195	0.96
GACFePo	298	51.179	1.446	0.0133	0.92	24.864	0.168	0.96
	308	65.866	0.3823	0.0382	0.89	27.936	0.195	0.94
	318	81.667	0.173	0.0661	0.94	28.134	0.236	0.94
GACFeMo	298	70.909	0.144	0.0892	0.95	24.642	0.216	0.96
	308	72.961	0.436	0.0305	0.97	31.760	0.193	0.96
	318	80.207	0.243	0.0488	0.98	29.056	0.231	0.91

$$k_d = \frac{q_e \times 0.05}{C_e \times 0.12} \quad (10)$$

The thermodynamic parameters of the three adsorbents are shown in Table 6. The negative values found for $\Delta G°$ for the three adsorbents indicate that the adsorption process of DCF occurs spontaneously and favourably with the increase in temperature. In addition, it is possible to observe that impregnation of the activated carbon with iron nanoparticles increased the degree of spontaneity for the three temperatures studied when compared with GAC.

The endothermic nature of the process is confirmed by the positive values of $\Delta H°$. As the values are lower than 40 kJ mol^{-1}, adsorption can be described as physisorption (Bekçi et al. 2007; Bhatnagar et al. 2010). As for $\Delta S°$, the positive values of GACFePo and GACFeMo reflect the increase in randomness at the liquid–solid interface during the adsorption of DCF. On the other hand, the GAC presented negative entropy values, indicating the accommodation of the adsorbate molecules in more ordered layers on the surface of the adsorbent.

Proposal of sodium diclofenac interactions on activated carbon adsorption

The mechanism of adsorption of DCF on the surface of activated carbon impregnated with iron oxide occurs possibly by a complex series of interactions between the functional groups of coal and iron oxide and the functional groups of diclofenac. Based on the analyses performed, as well as on kinetic tests and adsorption isotherms, it may be proposed that interactions of physisorption occur by electrostatic attraction (Fig. 11).

It is observed, however, that at pH 5 and 7, the adsorption maintains values very close to each other. However, at pH 10, the adsorption capacity decreases considerably. Thus, we must consider the different ionizations and charges presented by the adsorbent.

Regarding the possible interactions between DCF and iron oxide, it may be proposed that the carboxylic acid groups of DCF interact through complexation with the iron oxide ($FeOH^{2+}$) surface groups. This complexation can occur either by means of bidentate chelates or by bridged bidentate complexes (Zhao et al. 2017). Now at pH 10, the iron oxide is ionized in the FeO^- form; thus, repulsion occurs between these groups and the carboxyl of diclofenac.

Considering the hydrophobic character of DCF (pKa = 4.15) and its negative charge (pKa < pH), DCF adsorption is probably governed by π–π dispersive interactions with the two aromatic rings approaching the carbon surface and by attractive electrostatic forces with coal impregnated with iron oxide. However, other possible adsorption mechanisms may occur, including hydrogen bonds, or even chemisorption interactions with the impregnated iron oxides. A preferential sorption of DCF in iron oxides is also possible (Plakas and Karabelas 2016).

Table 6 Thermodynamic parameters of DCF adsorption by GAC, GACFePo, and GACFeMo

	$\Delta G°$ (kJ mol^{-1})			$\Delta H°$ (kJ mol^{-1})	$\Delta S°$ (kJ mol^{-1} K^{-1})
	T (K) = 298	T = 308	T = 318		
GAC	− 12.5355	− 12.6169	− 10.3687	1.4902	− 0.00353
GACFePo	− 13.4708	− 12.4832	− 11.5182	5.1201	0.011746
GACFeMo	− 15.1922	− 12.8247	− 12.050	5.1201	0.011746

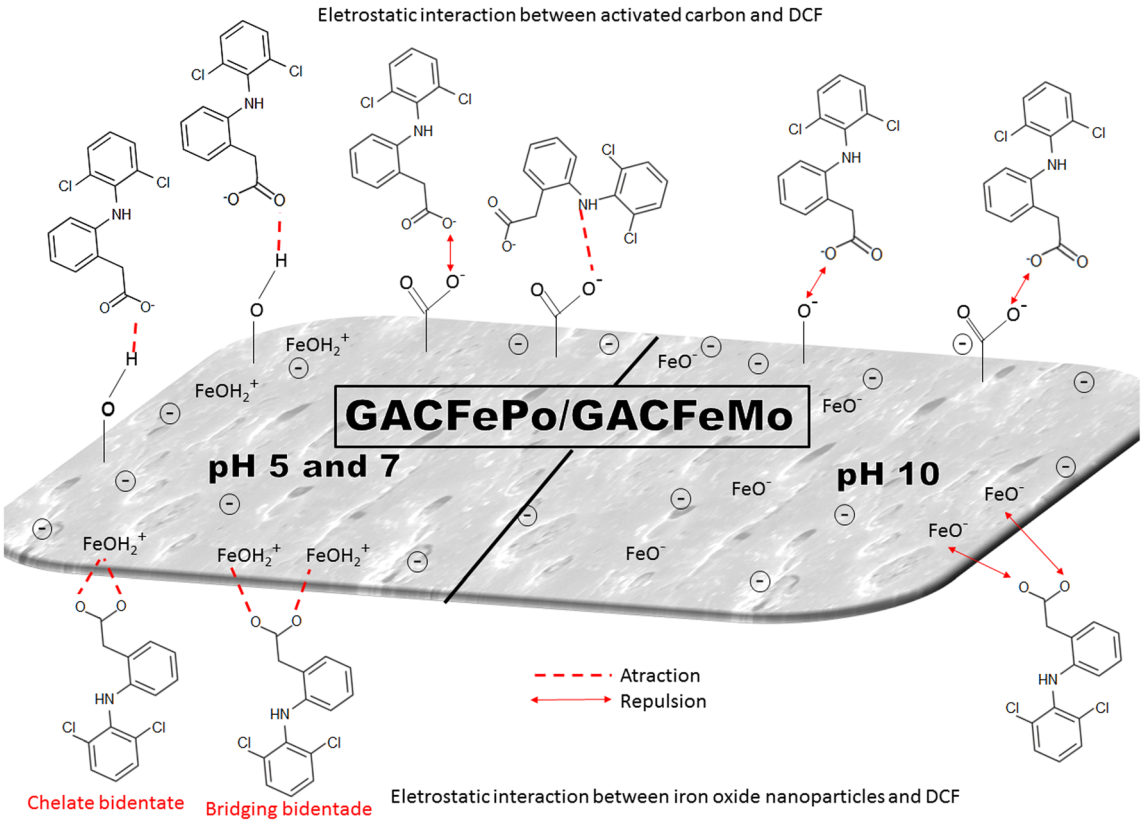

Fig. 11 Proposition of interactions for DCF adsorption in the studied adsorbents

Based on the combined characterization data of GACFePo and GACFeMo, as well as kinetic, equilibrium, and thermodynamic studies, it is also possible to suggest mechanisms of adsorption of DCF in activated carbon. The polar parts of DCF interact with the main functional groups of the adsorbent (OH, CO, COOH), as shown in Fig. 11. It can be assumed that at pH 5 and 7, electrostatic interactions occur between the hydroxyl and carboxyl groups of the coal and the carboxyl groups and amine of DCF. In addition, there are other interactions between the adsorbent and the DCF aromatic groups, as previously stated (Saucier et al. 2015). At pH 10, repulsion may occur between the carboxyl groups of DCF and the hydroxyl and carboxyl groups of the coal, all of which present negative charges at this pH. The magnitude of the adsorption enthalpy is in agreement with the physical forces of the attractions that exist between the adsorbent and the DCF.

Conclusions

In this work, the adsorbents were obtained by impregnation of iron oxide nanoparticles onto activated carbon by a green synthesis method using pomegranate and *Moringa* oleifera leaf extract and used for the removal of DCF from aqueous solution. The results showed that iron oxide nanoparticles in the goethite phase were successfully impregnated onto granular activated carbon. The adsorption process of DCF onto three adsorbents was fitted by the pseudo-second-order model. The adsorption isotherms fitted well with Langmuir and Freundlich models, depending on the temperature, and the q_{max} values obtained for the higher temperature (318 K) were 68.012, 80.207, and 81.667 mg g^{-1}, respectively, for GAC, GACFeMo, and GACFePo, which could be attributed to the strong interaction between DCF and goethite. It was observed that pH is a pronounced factor in the process; the adsorbents presented better removal in neutral medium, with a concentration of 100 mg L^{-1} DCF and a 120 mg mass of adsorbent. The adsorption thermodynamics indicated that the adsorption process was endothermic, and the adsorption was more favourable at higher temperatures.

References

Al-Hakeim HK, AL-Dahan IM, Al-Hillawi ZH, Bustan RS (2014) Interaction of prolactin hormone with the surfaces of two new azo compounds. Int J Pharm Pharm Sci 6:383–387

Bansal RC, Goyal M (2005) Activated carbon adsorption. CRC press, New York

Bekçi Z, Seki Y, Yurdakoç MK (2007) A study of equilibrium and FTIR, SEM/EDS analysis of trimethoprim adsorption onto K10. J Mol Struct 827:67–74. https://doi.org/10.1016/j.molstruc.2006.04.054

Bhatnagar A, Kumar E, Sillanpää M (2010) Nitrate removal from water by nano-alumina: characterization and sorption studies. Chem Eng J 163:317–323. https://doi.org/10.1016/j.cej.2010.08.008

Boukhalfa N, Boutahala M, Djebri N (2017) Synthesis and characterization of ZnAl-layered double hydroxide and organo-K10 montmorillonite for the removal of diclofenac from aqueous solution. Adsorpt Sci Technol 35:20–36. https://doi.org/10.1177/0263617416666548

Choi KJ, Kim SG, Kim CW, Park JK (2006) Removal efficiencies of endocrine disrupting chemicals by coagulation/flocculation, ozonation, powdered/granular activated carbon adsorption, and chlorination. Korean J Chem Eng 23:399–408. https://doi.org/10.1007/BF02706741

Collier AC (2007) Pharmaceutical contaminants in potable water: potential concerns for pregnant women and children. EcoHealth 4:164–171. https://doi.org/10.1007/s10393-007-0105-5

Cornell RM, Sshwertmann U (2003) The iron oxides: structures, properties, reactions, occurrences and uses. Wiley-VCH, Weinheim

Darezereshki E, Bakhtiari F, Vakylabad AB, Hassani Z (2013) Single-step synthesis of activated carbon/γ-Fe2O3 nano-composite at room temperature. Mater Sci Semicond Process 16:221–225. https://doi.org/10.1016/j.mssp.2012.08.007

Daves JW (2003) Current protocols in food analytical chemistry. John Wiley & Sons Inc. 1073–1080

Dos Santos JM, Pereira CR, Foletto EL, Dotto GL (2019) Alternative synthesis for ZnFe2O4/chitosan magnetic particles to remove diclofenac from water by adsorption. Int J Biol Macromol 131:301–308. https://doi.org/10.1016/j.ijbiomac.2019.03.079

Elfalleh W, Hannachi H, Tlili N, Yahia Y, Nasri N, Ferchichi A (2011) Total phenolic contents and antioxidant activities of pomegranate peel, seed, leaf and flower. J Med Plant Res 6:4724–4730. https://doi.org/10.5897/JMPR11.995

Fadavi A, Barzegar M, Azizi M, Bayat M (2005) Note. Physicochemical composition of ten pomegranate cultivars (Punica granatum L.) grown in Iran. Food Sci Technol Int 11:113–119. https://doi.org/10.1177/1082013205052765

Goscianska J, Nowak I, Nowicki P, Pietrzak R (2012) The influence of silver on the physicochemical and catalytic properties of activated carbons. Chem Eng J 189–190:422–430. https://doi.org/10.1016/j.cej.2012.02.069

Gulshan F, Kameshima Y, Nakajima A, Okada K (2009) Preparation of alumina-iron oxide compounds by gel evaporation method and its simultaneous uptake properties for Ni^{2+}, NH^{4+} and $H2PO^{4-}$. J Hazard Mater 169:697–702. https://doi.org/10.1016/j.jhazmat.2009.04.009

Ho Y, McKay G, Wase D, Forster C (2000) Study of the sorption of divalent metal ions on to peat. Adsorpt Sci Technol 18:639–650. https://doi.org/10.1260/0263617001493693

Hockridge JG, Jones F, Loan M, Richmond WR (2009) An electron microscopy study of the crystal growth of schwertmannite needles through oriented aggregation of goethite nanocrystals. J Cryst Growth 311:3876–3882. https://doi.org/10.1016/j.jcrysgro.2009.06.023

Huang L, Weng X, Chen Z, Megharaj M, Naidu R (2014) Green synthesis of iron nanoparticles by various tea extracts: comparative study of the reactivity. Spectrochim Acta A 130:295–301. https://doi.org/10.1016/j.saa.2014.04.037

Iliescu T, Baia M, Miclăuş V (2004) A Raman spectroscopic study of the diclofenac sodium–β-cyclodextrin interaction. Eur J Pharm Sci 22:487–495. https://doi.org/10.1016/j.ejps.2004.05.003

Iravani S (2011) Green synthesis of metal nanoparticles using plants. Green Chem 13:2638–2650. https://doi.org/10.1039/C1GC15386B

Islam MS, Ang BC, Gharehkhani S, Afifi ABM (2016) Adsorption capability of activated carbon synthesized from coconut shell. Carbon Lett 20:1–9. https://doi.org/10.5714/CL.2016.20.001

Jimoh TO (2018) Enzymes inhibitory and radical scavenging potentials of two selected tropical vegetable (Moringa oleifera and Telfairia occidentalis) leaves relevant to type 2 diabetes mellitus. Ver Bras Farmacogn 28:73–79. https://doi.org/10.1016/j.bjp.2017.04.003

Jodeh S, Abdelwahab F, Jaradat N, Warad I, Jodeh W (2016) Adsorption of diclofenac from aqueous solution using Cyclamen persicum tubers based activated carbon (CTAC). J Assoc Arab Univ Basic Appl Sci 20:32–38. https://doi.org/10.1016/j.jaubas.2014.11.002

Jorgensen SE, Halling-Sorensen B (2000) Drugs in the environment. Chemosphere 40:691–699. https://doi.org/10.1016/S0045-6535(99)00438-5

Khatami M, Alijani HQ, Fakheri B, Mobasseri MM, Heydarpour M, Farahani ZK, Khan AU (2019) Super-paramagnetic iron oxide nanoparticles (SPIONs): greener synthesis using Stevia plant and evaluation of its antioxidant properties. J Clean Prod 208:1171–1177. https://doi.org/10.1016/j.jclepro.2018.10.182

Kobayashi A, Gulshan F, Kameshima Y, Nnakajima A, Okada K (2008) Preparation and simultaneous ion uptake properties of CaO-Fe2O3-SiO2 compounds. J Ceram Soc Jpn 116:187–191. https://doi.org/10.1016/j.jclepro.2014.06.084

Koch CC, Ovid'Ko IA, Seal S, Veprek S (2007) (2007) Structural nanocrystalline materials: fundamentals and applications. Cambridge University Press. https://doi.org/10.1017/CBO9780511618840.008

Kumar VS, Nagaraja BM, Shashikala V, Padmasri AH, Madhavendra SS, Raju BD, Rao KS (2004) Highly efficient Ag/C catalyst prepared by electro-chemical deposition method in controlling microorganisms in water. J Mol Catal A Chem 223:313–319. https://doi.org/10.1016/j.molcata.2003.09.047

Kümmerer K (2009) The presence of pharmaceuticals in the environment due to human use–present knowledge and future challenges. J Environ Manag 90:2354–2366. https://doi.org/10.1016/j.jenvman.2009.01.023

Lam FLY, Hu X (2003) A new system design for the preparation of copper/activated carbon catalyst by metal-organic chemical vapor deposition method. Chem Eng Sci 58:687–695. https://doi.org/10.1016/S0009-2509(02)00596-1

Largergren S (1898) Zur theorie der sogenannten adsorption geloster stoffe. K Sven Vetenskapsakad Handl 24:1–39

Larous S, Meniai A-H (2016) Adsorption of diclofenac from aqueous solution using activated carbon prepared from olive stones. Int J Hydrog Energy 41:10380–10390. https://doi.org/10.1016/j.ijhydene.2016.01.096

Limousin G, Gaudet JP, Charlet L, Szenknect S (2007) Sorption isotherms: a review on physical bases, modeling and measurement. Appl Geochem 22:249–275. https://doi.org/10.1016/j.apgeochem.2006.09.010

Lonappan L, Rouissi T, Brar Satinder K, Verma M, Surampalli RY (2018) Adsorption of diclofenac onto different biochar microparticles: dataset – characterization and dosage of biochar. Data Brief 16:460–465. https://doi.org/10.1016/j.dib.2017.10.041

Nasri NS, Basri H, Garba A, Hamza UD, Mohammed J, Musa AM (2014) Synthesis and characterization of low-cost porous carbon from palm oil shell via K_2CO_3 chemical activation process. Appl Mech Mater 735:36–40. https://doi.org/10.4028/www.scientific.net/AMM.735.36

Njagi EC, Huang H, Stafford L, Genuino H, Galindo HM, Collins JB, Hoag GE, Suib SL (2010) Biosynthesis of iron and silver nanoparticles at room temperature using aqueous sorghum bran extracts. Langmuir 27:264–271. https://doi.org/10.1021/la103190n

Olabode Z, Akanbi C, Olunlade B, Adeola A (2015) Effects of drying temperature on the nutrients of Moringa (Moringa oleifera) leaves and sensory attributes of dried leaves infusion. World J Food Sci Technol 3:93–96. https://doi.org/10.11648/j.wjfst.20170103.11

Park S-J, Jang Y-S (2003) Preparation and characterization of activated carbon fibers supported with silver metal for antibacterial behavior. J Colloid Interface Sci 261:238–243. https://doi.org/10.1016/S0021-9797(03)00083-3

Philip D (2009) Biosynthesis of Au, Ag and Au–Ag nanoparticles using edible mushroom extract. Spectrochim Acta A 73:374–381. https://doi.org/10.1016/j.saa.2009.02.037

Plakas KV, Karabelas AJ (2016) A study on heterogeneous Fenton regeneration of powdered activated carbon impregnated with iron oxide nanoparticles. Global NEST J 18:259–268. https://doi.org/10.30955/gnj.001894

Prasad C, Karlapudi S, Venkateswarlu P, Bahadur I, Kumar S (2017) Green arbitrated synthesis of Fe_3O_4 magnetic nanoparticles with nanorod structure from pomegranate leaves and Congo red dye degradation studies for water treatment. J Mol Liq 240:322–328. https://doi.org/10.1016/j.molliq.2017.05.100

Qin TC, Song M, Jiang K, Zhou J, Zhuang W, Chen Y, Liu D, Chen X, Ying H, Wu J (2017) Efficient decolorization of citric acid fermentation broth using carbon materials prepared from phosphoric acid activation of hydrothermally treated corncob. R Soc Chem 7:37112–37121. https://doi.org/10.1039/C7RA04813K

Rai P, Gautam RK, Banerjee S, Rawat V, Chattopadhyaya MC (2015) Synthesis and characterization of a novel $SnFe_2O_4$@activated carbon magnetic nanocomposite and its effectiveness in the removal of crystal violet from aqueous solution. J Environ Chem Eng 3:2281–2291. https://doi.org/10.1016/j.jece.2015.08.017

Santos TR, Silva MF, Nishi L, Vieira AM, Fagundes-Klen MR, Andrade MB, Vieira MF, Bergamasco R (2016) Development of a magnetic coagulant based on Moringa oleifera seed extract for water treatment. Environ Sci Pollut Res 23:7692–7700. https://doi.org/10.1007/s11356-015-6029-7

Saucier C, Adebayo MA, Lima EC, Cataluna R, Thue PS, Prola LD et al. (2015) Microwave-assisted activated carbon from cocoa shell as adsorbent for removal of sodium diclofenac and nimesulide from aqueous effluents. J Hazard Mater 289:18–27

Schriks M, Heringa MB, van der Kooi MME, de Voogt P, van Wezel AP (2010) Toxicological relevance of emerging contaminants for drinking water quality. Water Res 44:461–476. https://doi.org/10.1016/j.watres.2009.08.023

Schwertmann U, Cornell RM (2008) Iron oxides in the laboratory: preparation and characterization. John Wiley & Sons

Shahwan T, Abu Sirriah S, Nairat M, Boyacı E, Eroğlu AE, Scott TB, Hallam KR (2011) Green synthesis of iron nanoparticles and their application as a Fenton-like catalyst for the degradation of aqueous cationic and anionic dyes. Chem Eng J 172:258–266. https://doi.org/10.1016/j.cej.2011.05.103

Silva AM, Santos OAA, Mendes MJ, Jordão E, Fraga MA (2003) Hydrogenation of citral over ruthenium-tin catalysts. Appl Catal A 241:155–165. https://doi.org/10.1016/S0926-860X(02)00463-5

Silva AM, Santos OAA, Morales MA, Baggio-Saitovitch EM, Jordão E, Fraga MA (2006) Role of catalyst preparation on determining selective sites for hydrogenation of dimethyl adipate over $RuSn/Al_2O_3$. J Mol Catal A Chem 253:62–69. https://doi.org/10.1016/j.molcata.2006.03.005

Singleton VL, Rossi JA (1965) Colorimetry of total phenolics with phosphomolybdic-phosphotungstic acid reagents. Am J Enol Vitic 16:144–158

Sotelo JL, Ovejero G, Rodríguez A, Álvarez S, Galán J, García J (2014) Competitive adsorption studies of caffeine and diclofenac aqueous solutions by activated carbon. Chem Eng J 240:443–453. https://doi.org/10.1016/j.cej.2013.11.094

Srinivasan NR, Shankar PA, Bandyopadhyaya R (2013) Plasma treated activated carbon impregnated with silver nanoparticles for improved antibacterial effect in water disinfection. Carbon 57:1–10. https://doi.org/10.1016/j.carbon.2013.01.008

Thakkar KN, Mhatre SS, Parikh RY (2010) Biological synthesis of metallic nanoparticles. Nanomedicine 6:257–262. https://doi.org/10.1016/j.nano.2009.07.002

Thommes M, Kaneko K, Neimark AV, Olivier JP, Rodriguez-Reinoso F, Rouquerol J, Sing KSW (2015) Physisorption of gases, with special reference to the evaluation of surface area and pore size distribution (IUPAC Technical Report). Pure Appl Chem 87:1051–1069

Uchimiya M (2014) Influence of pH, ionic strength, and multidentate ligand on the interaction of CdII with biochars. ACS Sustain Chem Eng 2(8):2019–2027

Venkata Ramana DK, Yu JS, Seshaiah K (2013) Silver nanoparticles deposited multiwalled carbon nanotubes for removal of Cu (II) and Cd (II) from water: surface, kinetic, equilibrium, and thermal adsorption properties. Chem Eng J 223:806–815. https://doi.org/10.1016/j.cej.2013.03.001

Viuda MM, Fernández LJ, Pérez ÁJ (2010) Pomegranate and its many functional components as related to human health: a review. Compr Rev Food Sci Food Saf 9:635–654

Vyas S, Kachhwaha S, Kothari S (2015) Comparative analysis of phenolic contents and total antioxidant capacity of Moringa oleifera Lam. Pharm J 7:1–8. https://doi.org/10.5530/pj.2015.7.5

Wang W, Xiao K, He T, Zhu L (2015) Synthesis and characterization of Ag nanoparticles decorated mesoporous sintered activated carbon with antibacterial and adsorptive properties. J Alloys Compd 647:1007–1012. https://doi.org/10.1016/j.jallcom.2015.05.180

Wiśniewska M, Nowicki P, Nosal-Wiercińska A, Pietrzak R, Szewczuk-Karpisz K, Ostolska I, Sternik D (2017) Adsorption of poly (acrylic acid) on the surface of microporous activated carbon obtained from cherry stones. Colloids Surf A Physicochem Eng Asp 514:137–145. https://doi.org/10.1016/j.colsurfa.2016.11.053

Yoon Y, Westerhoff P, Snyder SA, Wert EC, Yoon J (2007) Removal of endocrine disrupting compounds and pharmaceuticals by nanofiltration and ultrafiltration membranes. Desalination 202:16–23. https://doi.org/10.1016/j.desal.2005.12.033

Zhang S, Fu R, Wu D, Xu W, Ye Q, Chen Z (2004) Preparation and characterization of antibacterial silver-dispersed activated carbon aerogels. Carbon 42:3209–3216. https://doi.org/10.1016/j.carbon.2004.08.004

Zhang X, Lin S, Chen Z, Megharaj M, Naidu R (2011) Kaolinite-supported nanoscale zero-valent iron for removal of Pb2+ from aqueous solution: reactivity, characterization and mechanism. Water Res 45:3481–3488. https://doi.org/10.1016/j.watres.2011.04.010

Zhang Z, Li Y, Chen H, Zhang X, Li H (2018) The systematic adsorption of diclofenac onto waste red bricks functionalized with iron oxides. Water 10:1343–1355. https://doi.org/10.3390/w10101343

Zhao Y, Liu F, Qin X (2017) Adsorption of diclofenac onto goethite: adsorption kinetics and effects of pH. Chemosphere 180:373–378. https://doi.org/10.1016/j.chemosphere.2017.04.007

Zibin P., Yuman L., Binoy S., Gary O., Zuliang C., (2019) Green synthesis of iron nanoparticles using red peanut skin extract: synthesis mechanism, characterization and effect of conditions on chromium removal. Journal of Colloid and Interface Science, Elsevier BV. https://doi.org/10.1016/j.jcis.2019.09.106